J. Fluid Mech. (1971), *vol.* 47, *part* 3, *pp.* 577–599
Printed in Great Britain

A study of the constant-temperature hot-wire anemometer

By A. E. PERRY AND G. L. MORRISON

Mechanical Engineering Department,
University of Melbourne, Australia

(Received 14 April 1970)

The conventional 'bridge–feedback amplifier' constant-temperature hot-wire anemometer is analysed to determine its static and dynamic response. The effects of moderate feedback amplifier gain, bridge imbalance, stray bridge reactance, amplifier offset voltage, lack of common mode rejection, amplifier frequency response and departure from constant transconducture are included. The root loci of the system are mapped out and the consequences of the analysis are discussed from the viewpoint of both the operator and the designer.

1. Introduction

The hot-wire anemometer is an instrument which is usually calibrated statically and then used to measure quantities which have high-frequency components. The only way in which the experimentalist knows whether his instrument is operating correctly at high frequencies is to carry out a direct velocity perturbation test at these frequencies. This is difficult and inconvenient. Instead, the system response is inferred from an indirect electronic test such as exciting the system from an external voltage source. From the experimentalist's viewpoint this is unsatisfactory, especially when one considers the lack of any comprehensive account of the electronic behaviour of these systems. Commercial operating instruction manuals do not always give an insight into the processes occurring in the apparatus provided. As a result many users have little confidence in the results obtained.

The unsatisfactory state of hot-wire anemometry was made even more apparent to the authors when they found a lack of agreement between the turbulence levels indicated by different hot-wire systems for the measurement of the same flow (20 % difference in u') and when great difficulty was encountered in maintaining system stability. For these reasons, a detailed study of hot-wire anemometry was carried out and this paper reports on the first phase of the work. This is concerned with the behaviour of the standard bridge and feedback amplifier system.

With the increasing availability of cheap low drift operational amplifiers in integrated circuit form it is becoming easier for the non-electronic specialist to construct his own hot-wire anemometer. The authors hope that this paper will provide useful guide lines for the various adjustments which should be incorporated for proper operation and calibration of these systems.

In the past these systems have been designed to approach an apparent ideal situation where the wire is maintained at a constant temperature (hence its name). Under these conditions the wire is believed to follow certain known heat transfer laws. The temperature of the wire is never really constant and in any case if the system is appropriately calibrated the temperature variations are taken into account.

Attempts to maintain the wire temperature constant within very close limits by the use of high amplifier gain lead to problems in stability. Further incentives for the use of higher amplifier gain and hence constant wire resistance are: (1) the analysis of the system is greatly simplified, and (2) high-frequency response is believed to result. The usual simplified analysis assumes that the bridge is perfectly balanced at the operating point, and, if there are no stray reactances in the bridge, the impedance seen by the amplifier can be regarded as resistive and constant, thus leading to the idea of a constant-transconductance amplifier in a single feedback loop. This treatment omits many reasons for the observed instabilities. Hence an analysis is undertaken in which the effects of moderate amplifier gain, bridge imbalance, stray bridge reactance, amplifier offset voltage, lack of common mode rejection, amplifier frequency response and departure from constant transconductance are all included. To the authors' knowledge no similar comprehensive analysis has been published, although some analyses have included one or another of the above effects singly.

In §2 of this paper the static non-linear analysis is reported. The linearized dynamic analysis of an ideal system is reported in §4 and the connexion between the static and the dynamic analyses is shown. In §6 the stability and frequency response of a real hot-wire system are shown to be influenced by bridge reactance, and various practical complications are analysed. In §7 some experiments are reported which verify certain aspects of the analysis.

2. Static non-linear analysis

A typical circuit is shown in figure 1. The first stage is a differential amplifier of voltage gain K, with offset control. The second stage is a current booster with unity voltage gain. The amplifier used in such a system has the following ideal static behaviour:

$$E_0 = K(E_i + E_{qi}). \tag{1}$$

Here E_{qi} is the input offset voltage necessary to start the system operating and which may also be used to balance the bridge at some desired point. The output current from the amplifier is

$$I_0 = K(E_i + E_{qi})/R_T, \tag{2}$$

where R_T is the static resistance of the bridge. The component of I_0 which passes through the hot wire is

$$I_1 = I_0(R_b + R_c)/\Sigma R, \tag{3}$$

where

$$\Sigma R = R_a + R_b + R_c + R_w.$$

The amplifier input voltage is

$$E_i = I_1 R_a - I_2 R_c \tag{4}$$

$$= -I_0 \mathring{R}/\Sigma R, \tag{4a}$$

where $$\mathring{R} = R_w R_c - R_a R_b. \tag{4b}$$

Combining (2), (3) and (4) gives

$$I_1 = \frac{K E_{qi}(R_b + R_c)}{(R_a + R_w)(R_b + R_c) + K\mathring{R}}. \tag{5}$$

The static behaviour of the hot-wire element is

$$I_1^2 = F(U)(R_w - R_g)/R_w, \tag{6}$$

where R_g is the wire resistance at ambient temperature and U is the fluid velocity. There is some doubt about the precise form of $F(U)$. The 'King's law' form is

$$F(U) = X + Y\sqrt{U}, \tag{7}$$

where X and Y are constants dependent on the wire and fluid properties.† This may be only an approximate law but as far as the electronic analysis is concerned a different form of $F(U)$ would only make slight numerical differences to the

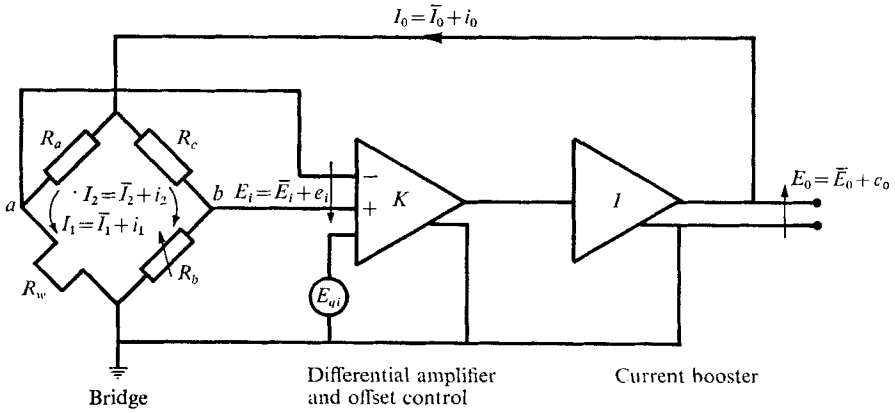

FIGURE 1. Constant-temperature hot-wire anemometer circuit elements. Typically $R_a = 100\ \Omega$, $R_b = 100\ \Omega$, $R_c = 1000\ \Omega$. R_w will be close to $10\ \Omega$.

system time constants and sensitivity. An operating point of special interest is at bridge balance and this will be referred to as the balance point. For this situation

$$E_i = 0, \quad \mathring{R} = 0. \tag{8}$$

A convenient representation of the static operation of the closed-loop system is formed by a cross-plot of equations (5) and (6) as shown in figure 2. In this figure the operating point is defined by the intersection of (5) with K and E_{qi} constant and (6) with U constant. The vertical asymptote of (5) is

$$R_{wa} = \frac{KR_aR_b - R_aR_b - R_aR_c}{KR_c + R_b + R_c}. \tag{9}$$

For low gains (9) shows that the asymptotic resistance R_{wa} may be less than R_g. However, for this to occur (6) shows that I_1^2 must be negative, which implies that the wire is cooled by the current. Equation (6) asymptotes to $I_1^2 = \lambda = X + Y\sqrt{U}$ as $R_w \to \infty$. The broken curve is a solution of (5) for negative gain or negative

† For purposes of calculations throughout this paper adopted values for a typical platinum wire 4 μm diameter and 1·2 mm long in air are $X = 2300\ (\text{mA})^2$, $Y = 840\ (\text{mA})^2\ \text{s}^{\frac{1}{2}}\text{m}^{-\frac{1}{2}}$ and $R_y = 5\Omega$.

offset voltage. This path is not of interest since, as will be shown later, all points to the left of R_{wa} are unstable.

The static behaviour of the system may be understood by tracing the path of the operating point and balance point in figure 2 as the gain (K) and offset voltage (E_{qi}) are varied. Consider the system to be operating with a balanced bridge at point A. Suppose the offset voltage is reduced but R_b is varied so as to maintain bridge balance. As E_{qi} is reduced the balance point will move along the constant-velocity line $\sqrt{U_2}$ = const. (A, A', A'') until it reaches the point $R_w = R_g$. This adjustment reduces the wire current to zero and the system ceases to operate. During this adjustment the vertical asymptote for (5) shifts to $R_{wa} = R_g$. On a King's law plot as shown in figure 3 the path traced out is along a vertical line through the initial balance point A.

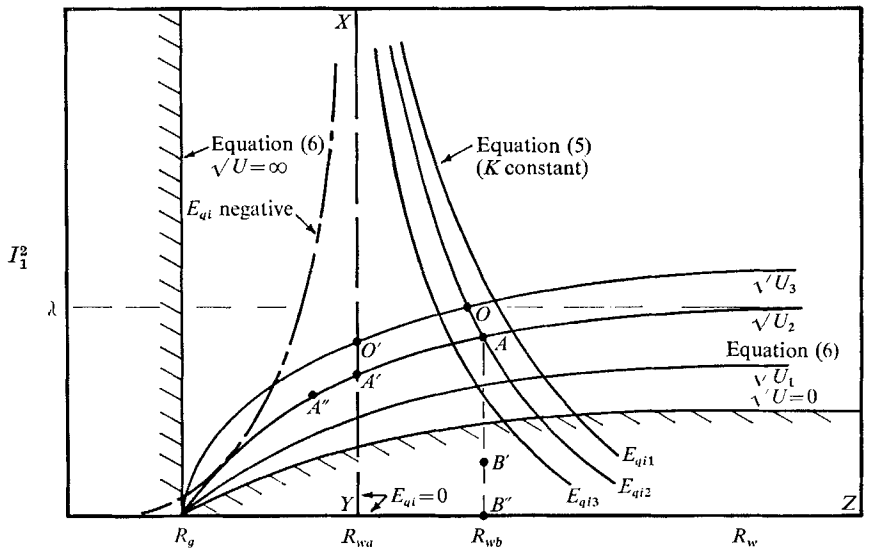

FIGURE 2. Amplifier and hot-wire characteristics.

The shaded lines in figure 3 represent the boundaries outside which the solution trajectories cannot go. The upper boundary is the infinite resistance line (see equation (6)) and represents the case of heat generation in the wire reaching the maximum limit which can be removed by the flow for the set of conditions imposed. Burnout will occur before this condition is reached.

Another method for shifting the balance point is to vary the velocity and offset voltage while the bridge resistors (R_a, R_b and R_c) are maintained fixed. If the former two quantities are varied in a way which maintains bridge balance the balance point in figure 2 moves along the vertical path $R_w = R_{wb}$, as the offset voltage is reduced. The points B' and B'' are 'virtual balance points' since for these $\sqrt{U} < 0$. A corresponding 'virtual balance point' is shown as point B' in figure 3. This point is outside the region of possible solutions and means, physically, that the system-operating point can never correspond with a virtual balance point.

A third method of varying the balance point is to hold the velocity and bridge resistors (R_a, R_b, R_c) constant while E_{qi} is varied. The balance point (initially

point A in figure 2) will move along the vertical line $R_w = R_{wb}$. The system-operating point O will move along the curve $\sqrt{U_3}$ = constant. When $E_{qi} = 0$, (5) is represented by the lines XY and YZ and the balance point is B'' and the operating point O'. The operating point and balance point will coincide when point O meets the vertical line $R_w = R_{wb}$. This occurs somewhere between E_{qi1} and E_{qi2}.

The third technique is the most practical means of adjusting the balance point. As a result of this adjustment, E_{qi} may approach zero while the current remains finite and for this situation the right-hand side of (5) must be indeterminate. Hence

$$(R_a + R_w)(R_b + R_c) + K\mathring{R} = 0. \tag{10}$$

In §4.1 this limiting process will be shown to be important in determining the frequency response and stability of an ideal hot-wire system. Figure 2 also indicates that as the velocity is varied the operating point moves along a path

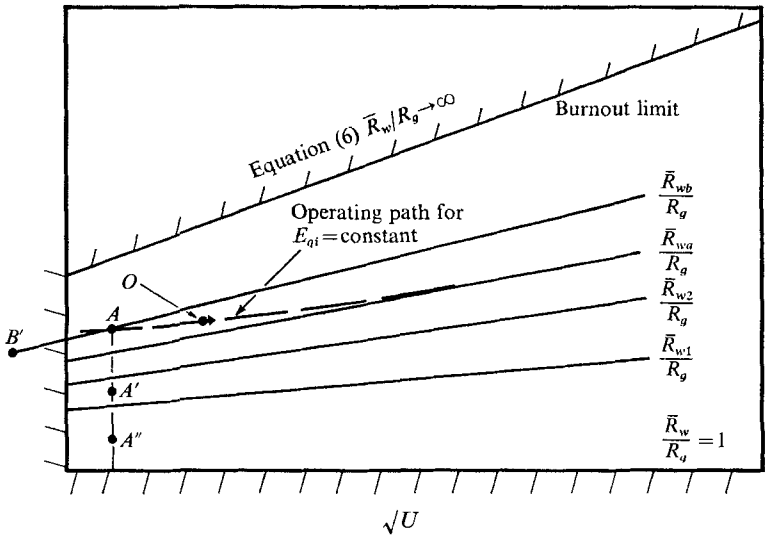

FIGURE 3. King's law plot.

defined by E_{qi} = constant. Thus, as $\sqrt{U} \to \infty$, the wire resistance R_w asymptotes to a limiting value R_{wa}. On a King's law plot in figure 3 the path traced out by the operating point is shown by the broken line. The amount by which this path varies from a constant resistance line will depend on the gain and offset voltage of the feedback amplifier. The variation of wire resistance causes the local slope of the calibration data, I_1^2 *vs.* $\sqrt{U}$, to be a function of velocity. This affects the dynamic sensitivity and will be discussed further in §6.6.

3. Linearized d.c. perturbation response of the hot wire

The system will be analysed by linearizing around the operating point as defined in the static analysis. The hot wire is a non-linear device whose voltage–current characteristic may be determined from (6) as

$$E_w = R_g F(U) I_1 / (F(U) - I_1^2). \tag{11}$$

Also $E_w = R_w I_1$ by definition of R_w. The form of (11) for constant velocity, that is, constant $F(U)$, is shown in figure 4. The slope of the graph at the origin is equal to the cold-wire static resistance R_g. At the operating point D, the static wire resistance is R_w and the d.c. small perturbation wire resistance is given by the tangent to the curve at D.

$$Z_{wdc} = \partial E_w / \partial I_1. \tag{12}$$

From (11) and (12)

$$Z_{wdc} = \bar{R}_w + \alpha, \tag{13}$$

where

$$\alpha = 2\bar{R}_w(\bar{R}_w - R_g)/R_g.$$

The overbar on R_w denotes values at the operating point D. For high currents or high wire temperatures the impedance given by (13) will differ greatly from the wire static resistance.

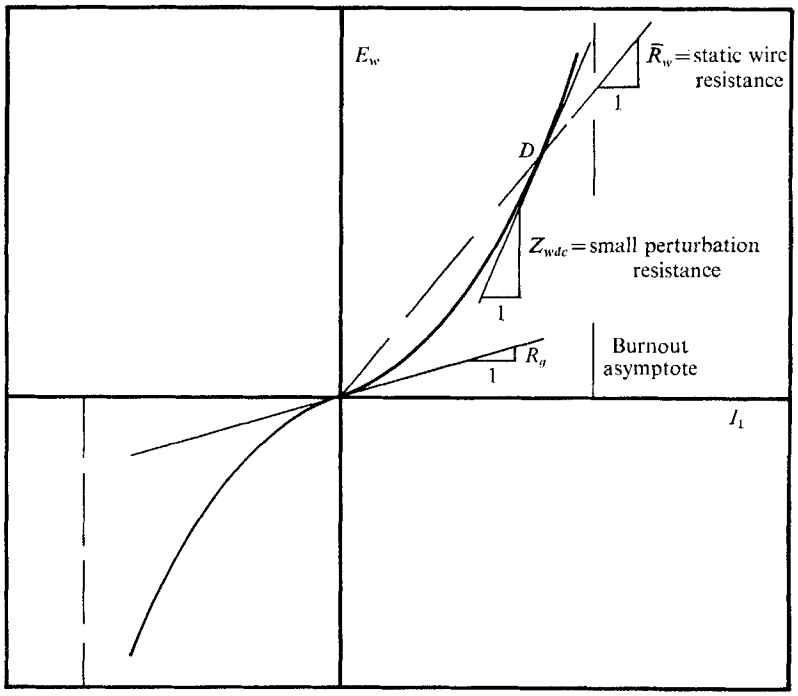

FIGURE 4. Voltage *vs.* current characteristic of hot wire.

4. Operation of an ideal hot-wire anemometer in a turbulent field

4.1. *Basic equations*

Throughout this paper upper-case letters, such as E_w, denote the instantaneous values of the various quantities. Overbars such as $\bar{E}_w$ denote temporal means, and lower-case letters such as e_w small perturbations. Thus $E_w = \bar{E}_w + e_w$. The same lower-case letters will also be used for the Laplace transforms of the perturbations.

The analysis presented here is applicable to an amplifier which has a flat response from d.c. to frequencies well beyond the range of interest. In §6.4 the effects of finite amplifier frequency response are investigated. Some hot-wire

systems have a very high d.c. or low frequency gain and a moderate and flat a.c. gain. The change in gain occurs at frequencies of the order of 100 Hz. The following analysis is applicable to a typical system shown in figure 1 if $K_{dc}/K_{ac} > 10$, $K_{ac} > 500$, K_{dc} is used in the calculation of $\mathring{R}$ and K_{ac} is used in the various perturbation equations in place of the symbol K.

The linearized approximation for the wire voltage perturbation e_w due to a velocity perturbation u' and a current perturbation i_1, is given by

$$e_w = u' \left.\frac{\partial E_w}{\partial U}\right|_{i_1=0} + i_1 \left.\frac{\partial E_w}{\partial I_1}\right|_{u'=0}. \tag{14}$$

The second term in (14) includes the effect of current changes generated by the feedback system attempting to maintain constant wire resistance. In this equation time derivatives do not enter since all analysis which follows is carried out in the frequency domain.

The sensitivity of the wire to velocity perturbations at constant current $(\partial E_w/\partial U)_{i=0}$ may be obtained from the dynamic energy balance relation for the wire. This relation is (6) with an additional term to allow for heat accumulation in the wire. The King's law form is

$$I_1^2 R_w = (R_w - R_g)(X + Y\sqrt{U}) + C(dR_w/dt). \tag{15}$$

The constants X and Y are obtained by experiment for a given wire and C depends on the thermal capacity of the wire.

From (15)
$$\left.\frac{\partial E_w}{\partial U}\right|_{i_1=0} = -\frac{x}{TS+1}, \tag{16}$$

where S is the Laplace variable,

$$x = \frac{Y(R_w - R_g)^2}{2\sqrt{U}\, R_g I_1} \quad \text{and} \quad T = \frac{C(R_w - R_g)}{I_1^2 R_g}.$$

T is the 'constant current' time constant due to the thermal capacity of the wire. This is also the time constant of a constant-current hot-wire anemometer without a compensation network. See Hinze (1959).

Similarly, the wire sensitivity to current perturbations at constant velocity may be obtained from (15):

$$\left.\frac{\partial E_w}{\partial I_1}\right|_{u'=0} = Z_w = \bar{R}_w + \frac{\alpha}{TS+1}. \tag{17}$$

$\bar{R}_w$ defines the operating point of R_w, and to the linearizing approximation the temporal mean value of R_w is equal to $\bar{R}_w$.

Equation (17) specifies the linearized hot-wire dynamic impedance, which is seen to be frequency dependent. This is a more general form of (13). The following equations describe the response of the typical system shown in figure 1:

$$e_0 = i_1 R_a + e_w, \tag{18}$$

$$e_0 = i_2(R_b + R_c), \tag{19}$$

$$e_i = i_1 R_a - i_2 R_c, \tag{20}$$

$$i_0 = i_1 + i_2, \tag{21}$$

and from (14), (16) and (17)

$$e_w = -u' \frac{x}{TS+1} + i_1 \frac{\alpha}{TS+1} + i_1 \bar{R}_w. \tag{22}$$

Equations (18) and (22) give

$$e_0 = -u' \frac{x}{TS+1} + i_1 \left(R_a + R_w + \frac{\alpha}{TS+1} \right). \tag{23}$$

An additional equation is required before the transfer function of the closed-loop system can be derived. This may be obtained by analysing the effect of bridge impedance variations on the amplifier output current by formulating the small signal equivalent circuit of the amplifier and bridge. The equivalent circuit of a transistorized amplifier system is given in figure 5. The equivalent circuit of the bridge must also be determined. Equations (19), (20) and (21) show

$$e_0 = \frac{i_0[\alpha + (\bar{R}_w + R_a)(TS+1)](R_b + R_c) - u'(R_b + R_c)x}{\Sigma R(TS+1) + \alpha}. \tag{24}$$

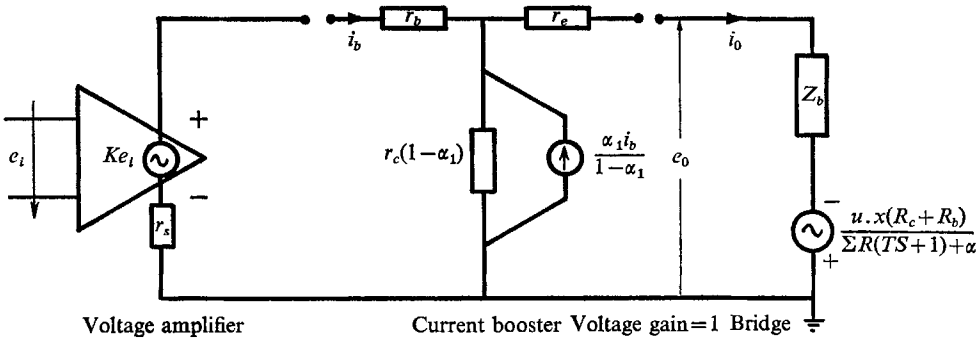

FIGURE 5. Amplifier and bridge equivalent circuits. r_s = amplifier output resistance; r_b = current booster input resistance; α_1 = transistor parameter; r_c = collector resistance; r_e = emitter resistance.

Using (17), the total bridge impedance Z_B is

$$Z_B = \frac{(R_c + R_b)[(R_a + \bar{R}_w)(TS+1) + \alpha]}{\Sigma R(TS+1) + \alpha}. \tag{25}$$

Combining (24) and (25),

$$e_0 = i_0 Z_B - \frac{u'(R_c + R_b)x}{\Sigma R(TS+1) + \alpha}. \tag{26}$$

Equation (26) gives the small signal equivalent circuit for the bridge as shown in figure 5. Investigation of this circuit using the usual transitor approximations† gives

$$i_0 = Ge_i + Hu', \tag{27}$$

where

$$G = K/Z_B, \quad H = (R_c + R_b)x/Z_B[\Sigma R(TS+1) + \alpha]. \tag{28}$$

Combining (20), (21), (22), (23) and (27) the transfer function between the input velocity perturbation and amplifier output voltage may be obtained:

$$e_0/u' = \frac{K_1}{(T_4 S+1)}, \tag{29}$$

† These approximations improve with multiple stages. Two stages are usually sufficient.

where T_4 is the system time constant and K_1 the sensitivity,

$$T_4 = \frac{[(R_b+R_c)(R_a+\bar{R}_w)+K\mathring{R}]T}{(R_b+R_c)(R_a+\bar{R}_w+\alpha)+K(\mathring{R}+R_c\alpha)}. \tag{30}$$

$$K_1 = \frac{KR_a(R_c+R_b)x}{(R_b+R_c)(R_a+\bar{R}_w+\alpha)+K(\mathring{R}+R_c\alpha)}. \tag{31}$$

The system gain $|e_0/u'|$ for sinusoidal inputs of frequency ω is equal to the modulus of (29) with $S = j\omega$, where $j = \sqrt{-1}$. Equations (29), (30) and (31) show that the dynamic and static responses are coupled through the term $\mathring{R} = \bar{R}_w R_c - R_a R_b$.

In §2 it was shown that if the offset voltage is reduced to zero while all other quantities were maintained constant then

$$(R_b+R_c)(R_a+\bar{R}_w)+K\mathring{R} = 0 \quad \text{(see equation (10))}.$$

From (10) and (30) it can be seen that the time constant is zero for zero offset. Thus the frequency response of a simple hot-wire system increases as the offset voltage is reduced. If E_{gi} is negative T_4 is negative and the system is unstable. Thus for stable performance the operating point must be to the right of the vertical line $\bar{R}_w = R_{wa}$ shown in figure 2.

The standard method of analysing a constant-temperature system is to assume that a very high gain amplifier is used. It is also usually assumed that: (1) the bridge is in perfect balance, $\mathring{R} = 0$; and (2) the bridge impedance seen by the amplifier is equal to the static bridge resistance with

$$Z_{wdc} = Z_{wac} = \bar{R}_w.$$

Thus the transconductance of the amplifier is given by

$$G = I_0/E_i = i_0/e_i|_{dc} = i_0/e_i|_{ac} = K/R_B. \tag{32}$$

Combining these assumptions with (20), (21), (23), (27) and (28) gives

$$\begin{aligned} T_4 &= \frac{T}{1+KR_c\alpha/[(R_b+R_c)(R_a+\bar{R}_w)]} \\ &= T/(1+GR_c\alpha/\Sigma R). \end{aligned} \tag{33}$$

This simplified relation may be shown to be the same as that derived by Hinze (1959).

Janssen, Ensing & Van Verp (1959), Grant & Kronauer (1962), Berger, Freymuth & Frobel (1963*a*, *b*), Anderson (1966) and Freymuth (1966) used the above assumptions in their analyses. Ossofsky (1948) assumed perfect bridge balance but included the effect of variable transconductance. Davis & Davies (1968) analysed the system using the second assumption. However, they omitted to derive the analytical connection between various parameters. The combination of the authors' static analysis with the dynamic analysis of Davis & Davies forms a closed set of equations. These equations and the exact equations derived here asymptote together for large gains. However, departure occurs for finite gains and low resistance ratios.

The following analysis will show that the assumption of perfect bridge balance is incorrect even for $K \to \infty$. If $\mathring{R}$ approaches zero as K is increased, (5) indicates that the wire current will increase without limit. However (6) shows that the wire

current is always below the asymptotic limit of $I_1^2 = \lambda = X + Y\sqrt{U}$. This demonstrates that if $\mathring{R}$ approaches zero as K is increased an inconsistency develops between the response of the feedback system (5) and the response of the hot wire (6). Equations (5) and (6) may be simultaneously satisfied for large and increasing K only if $\mathring{R}$ approaches a finite limit. This limit may be determined by equating the asymptotic form of (5) and (6) thus:

$$\left[\frac{E_{qi}(R_b+R_c)}{\mathring{R}}\right]^2 = \frac{\bar{R}_w - R_g}{\bar{R}_w}(X + Y\sqrt{U}). \tag{34}$$

For the typical circuit values shown in figure 1 the limiting asymptote for $\mathring{R}$ is of the order of $100\,\Omega^2$ for a typical wire with $U = 30\,\mathrm{ms}^{-1}$ and $E_{qi} = 10\,\mathrm{mV}$.

Thus the simplification made by assuming perfect bridge balance and ignoring the term $\mathring{R}$ leads to an incorrect expression for the system time constant and sensitivity. The magnitude of these errors will be demonstrated in §6.1.

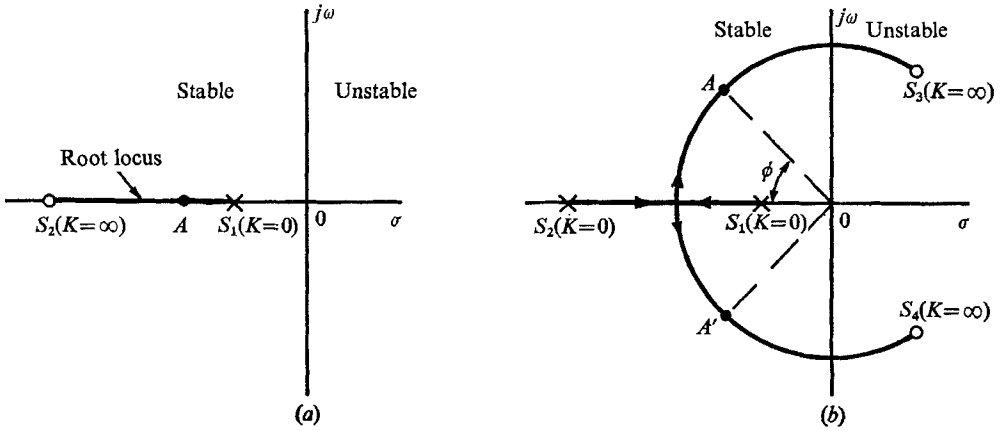

FIGURE 6. Typical root locus diagrams. (*a*) Simple anemometer. (*b*) Inductive anemometer. Damping coefficient $\zeta = \cos(\phi)$, frequency response = OA.

4.2. *Root locus of an ideal anemometer*

The stability and frequency response of a linear system may be specified by the root locus diagram. This is a plot on the S plane ($S = \sigma + j\omega$) of the system poles (values of S which give $|e_0/u'| = \infty$), for variation of amplifier gain (K) (see figure 6). The end-points S_1, S_2 etc. of the root loci are determined from the transfer function when expressed in the following form:

$$e_0/u' = H(S)/(1 - KG(S)/F(S)), \tag{35}$$

where $H(S)$, $F(S)$ and $G(S)$ are polynomials of the Laplace variable S.

The system response is governed by the characteristic equation

$$1 - KG(S)/F(S) = 0.$$

Solutions of this equation are called the system poles. The end points of the root locus are given by the zeros of $G(S)$ (values of S for which $G(S) = 0$) for $K = \infty$ and by the zeros of $F(S)$ for $K = 0$. When these limits are evaluated the position of the system poles for any gain K may be sketched in using the various root locus rules, see Horowitz (1963).

If the end points have positive real parts (i.e. occur in the positive half of the root locus diagram) the system will be unstable for amplifier gains represented by the section of the locus in the positive half-plane. The scalar distance of any pole from the origin is equal to the characteristic frequency of that pole. For the operating point A, in figure 6(a) the frequency response is equal to OA. If there is more than one pole the system frequency response or 'roll-off' frequency is defined as the lowest frequency of all the system poles. Although the system will respond to higher frequencies it is unusable beyond the first pole because for frequencies beyond this the system sensitivity varies with frequency.

If the poles are complex as shown in figure 6 the system has a second-order response and the frequency response is equal to OA ($= OA'$). The damping coefficient is equal to the cosine of the angle ϕ.

The terminal points of the root locus of an ideal anemometer may be evaluated by comparing (29) and (35).

For $K = 0$ $$S_1 = -(R_a + \bar{R}_w + \alpha)/(\bar{R}_a + \bar{R}_w)T. \tag{36}$$

For $K = \infty$ $$S_2 = -(\mathring{R} + R_c\alpha)/\mathring{R}T. \tag{37}$$

5. Experimental investigation of frequency response

A convenient experimental technique for determining the system frequency response is to apply small signal sine wave voltage perturbations from an external source. To achieve this the offset voltage may be modulated so that

$$E_{qi} = \bar{E}_{qi} + e_s \sin(\omega t). \tag{38}$$

The transfer function for this case may be derived in a manner similar to that used for velocity perturbations. This results in

$$e_0/e_s = KK_2(T_2'S + 1)/(T_4'S + 1), \tag{39}$$

where $$T_2' = (R_a + \bar{R}_w)/(R_a + \bar{R}_w + \alpha).$$

Equation (39) shows that the characteristic pole of the system for an external voltage signal (e_s) is the same as for a velocity perturbation input. Experimental investigation of constant-temperature hot-wire systems using external voltage signals showed that the actual response did not have the form of (39). Instead, a second- or higher-order response was observed. These higher-order effects occurred at frequencies well below the amplifier roll-off frequency. Further investigation revealed that they were due to bridge inductance. This was verified by adding small reactive elements to the bridge. Inductances of the order of microhenrys were found to shift the system frequency response by substantial amounts, whereas the addition of large capacitors had small effect. The most important source of inductance is the hot-wire cable.

6. Analysis of real hot-wire systems

6.1. *Analysis of hot wire with wire inductance*

To include the effect of wire inductance (23) must be modified to read

$$e_0 = -u' \frac{x}{TS+1} + i_1 \left[R_a + \bar{R}_w + SL_w + \frac{\alpha}{TS+1} \right], \tag{40}$$

where L_w is the wire inductance. Using the same technique as outlined earlier leads to

$$\frac{e_0}{u'} = \frac{K_1}{(S/\omega_n)^2 + 2\zeta(S/\omega_n) + 1}, \tag{41}$$

where

$$\frac{1}{\omega_n^2} = \frac{(R_c+R_b)L_wT + KR_cL_wT}{(R_b+R_c)(R_a+\bar{R}_w+\alpha) + K(\mathring{R}+R_c\alpha)},$$

$$\frac{2\zeta}{\omega_n} = \frac{(R_a+\bar{R}_w)(R_b+R_c)T + (R_c+R_b)L_w + K(\mathring{R}T+R_cL_w)}{(R_b+R_c)(R_a+\bar{R}_w+\alpha) + K(\mathring{R}+R_c\alpha)},$$

ω_n is the system natural frequency and ζ the damping coefficient. The roots of the characteristic equation may be either 'real' or 'complex' depending on the offset voltage, amplifier gain and inductance. To determine the frequency response and

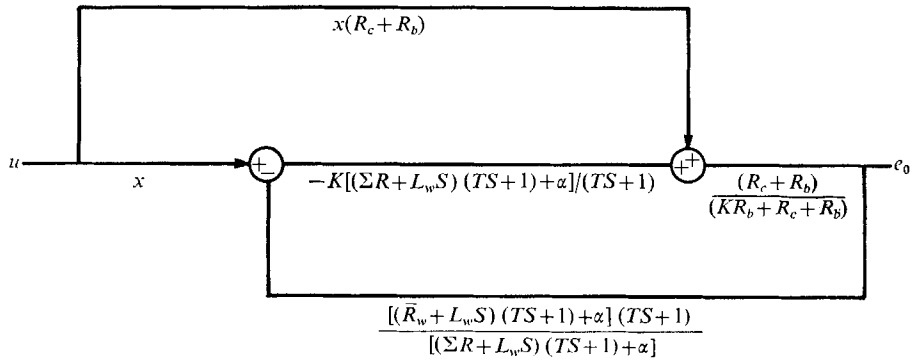

FIGURE 7. Signal flow chart of hot-wire anemometer with wire inductance.

stability, the root loci for this more complicated system will be determined. The signal flow chart formulated from (19), (20), (21), (27) and (40) is shown in figure 7. Derivation of the closed-loop transfer function using the method given in §4.2 shows that the terminal points of the loci for $K = 0$ are

$$S_{1,2} = \frac{-[(R_a+\bar{R}_w)T + L_w] \pm \{[(R_a+\bar{R}_w)T - L_w]^2 - 4L_wT\alpha\}^{\frac{1}{2}}}{2L_wT}. \tag{42}$$

The terminal points of the loci for $K = \infty$ are

$$S_{3,4} = \frac{-\mathring{R}T - R_cL_w \pm \{[-R_0T - R_cL_w]^2 - 4R_cL_wT(\mathring{R}+R_c\alpha)\}^{\frac{1}{2}}}{2L_wR_cT}. \tag{43}$$

Typical root loci are shown in figure 6. The loci were obtained using the usual root loci construction (see Horowitz 1963). These curves follow Laplace's equation. Using a hydrodynamic analogy the terminal points $K=0$ and $K=\infty$ correspond to unit strength sources and sinks respectively and the locus is given by the stream function $\psi = \frac{1}{2}$. The root locus representation is applicable to this system for fixed bridge imbalance only (constant $S_{1,2}$ and $S_{3,4}$). This is not a practical condition since $\mathring{R}$ is constant for varying K only if the offset E_{qi} is appropriately adjusted. Loci of more interest are those for fixed E_{qi}. Under these conditions the 'end points' given by (42) and (43) vary with K and the loci do not follow Laplace's equation. The terminal points for this more practical class of

loci can be obtained from (42) and (43), with $\mathring{R}$ equal to its limiting value given by (34).

The actual loci for fixed E_{qi} were obtained by numerical calculation of the roots of (41) for varying K with the aid of (4*b*), (5) and (6) for calculating R_w and R. The results of these calculations non-dimensionalized with T are shown in figure 8. Also shown are contours of K. Figure 9 shows the loci of the terminal points for varying input offset. The parameters which are to be varied in order to

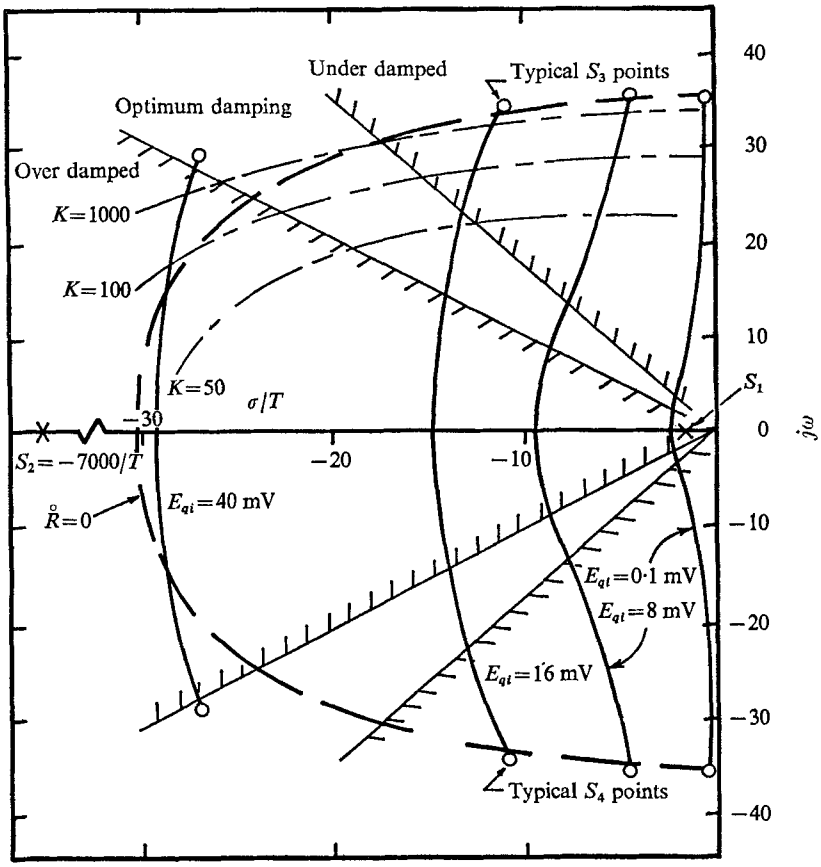

FIGURE 8. Operating-point trajectories of inductive hot-wire anemometer with constant input offset voltage. $L_w = 5\mu$H, $\bar{U} = 30$ ms^{-1}.

obtain optimum response are evident. The results of the usual root loci construction using the terminal points given by (42) and (43) for $\mathring{R} = 0$ are shown by the heavy broken curve in figure 8. This is the path of the system poles obtained from the assumption of perfect bridge balance at all operating points.

6.2. *Experimental investigation of second-order response*

The response of a hot-wire system with inductance, to an external voltage signal, is

$$\frac{e_0}{e_s} = \frac{K_2\left[\dfrac{L_w T}{R_a+\bar{R}_w+\alpha}S^2+\dfrac{(R_a+\bar{R}_w)T+L_w}{R_a+\bar{R}_w+\alpha}S+1\right]}{(S/\omega_n)^2+2\zeta(S/\omega_n)+1}, \tag{44}$$

where ω_n and ζ are given by (41). The numerator of (44) factorizes to give two real zeros, one at a frequency well beyond the range of interest, typically $T_6 = T/1500$, and the other close to the zero in the system without wire inductance. Equation

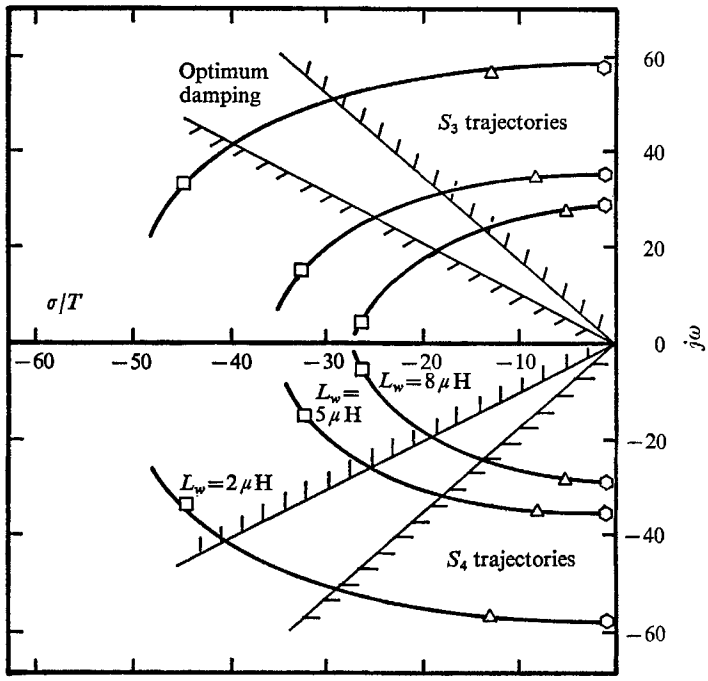

FIGURE 9. S plane trajectories of terminal points for varying offset voltage: ⬡, 0 mV; △, 10 mV; □, 30 mV, $\bar{U} = 30\,\mathrm{ms}^{-1}$.

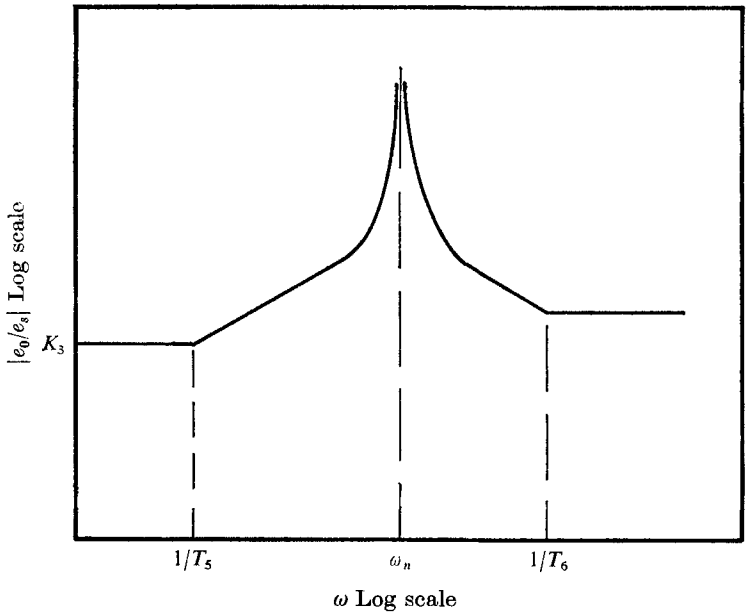

FIGURE 10. Bode diagram for current injection.

(44) is shown on a Bode diagram in figure 10, where T_5 is the lower frequency time constant in the numerator. The peaking at $\omega = \omega_n$ will depend on the offset voltage and for some cases the poles may have real components only.

6.3. *Improvement of frequency response of the hot-wire system*

Analysis of a system with an additional variable inductor L_b in the bridge arm opposite the hot wire shows that the quadratic poles still occur but the natural frequency may be increased. A similar behaviour is obtained if the additional inductor is placed in the same side of the bridge as the hot wire.

The form of the response for L_b in the same arm as R_b is

$$\frac{e_0}{u'} = \frac{K_1(E_1 S + 1)}{A_1 S^3 + B_1 S^2 + C_1 S + 1}, \tag{45}$$

where

$$E_1 = \frac{L_b}{R_b + R_c}, \quad A_1 = \frac{L_b L_w T}{(R_b + R_c)(R_a + \bar{R}_w + \alpha) + K(\mathring{R} + R_c\alpha)},$$

$$B_1 = \frac{L_b[(R_a + \bar{R}_w)T + L_w] + L_w T(R_b + R_c) - K[R_a L_b - R_c L_w]T}{(R_b + R_c)(R_a + \bar{R}_w + \alpha) + K(\mathring{R} + R_c\alpha)},$$

$$C_1 = \frac{L_b(R_a + \bar{R}_w + \alpha) + L_w(R_b + R_c) + (R_a + \bar{R}_w)(R_b + R_c)T - K(R_a L_b - R_c L_w - \mathring{R}T)}{(R_b + R_c)(R_a + \bar{R}_w + \alpha) + K(\mathring{R} + R_c\alpha)}.$$

Typically the denominator of (45) factorizes to give one real pole and one 'complex' pair of poles. The real pole and the zero are generally well above the range of interest. For the typical values listed in figure 1 (45) predicts that if L_b is increased from 0 to 30 μH the natural frequency at zero mean velocity will increase from 10 kHz to 40 kHz. Experimental investigation using a square-wave voltage signal showed an improvement of this order.

Analysis of the system with inductors in both sides of the bridge indicates that the terminal points of the root loci are:

for $K = 0$
$$S_3 = -(R_c + R_b)/L_b, \tag{46}$$

$$S_{4,5} = \frac{-[(R_a + R_w)T + L_w] \pm \{[(R_a + \bar{R}_w)T - L_w]^2 - 4L_w T\alpha\}^{\frac{1}{2}}}{2L_w T}, \tag{47}$$

or $K = \infty$

$$S_{6,7} = \frac{\mathring{R}T + R_c L_w - R_a L_b \pm \{[-\mathring{R}T - R_c L_w + R_a L_b]^2 - 4(R_c L_w T - R_a L_b T)(\mathring{R} + R_c\alpha)\}^{\frac{1}{2}}}{2[R_a L_b - R_c L_w]T}. \tag{48}$$

The loci of the system singularities for varying bridge balance were obtained by numerical calculation of the roots of (45). The values of the terminal points were obtained from (46), (47) and (48) using the asymptotic value of $\mathring{R}$ as given by (34). The results non-dimensionalized with T are shown in figure 11. The broken curve is the path which would be predicted by authors who assume bridge balance at all operating points. Figure 11 indicates which gains and offset voltages are required for optimum damping, i.e. $0{\cdot}55 < \zeta < 0{\cdot}65$. Figure 12 shows

the path of the operating point for varying L_b and the loci of the terminal points for varying offset voltage are shown in figure 13.

Equation (48) shows that the frequency response is a maximum when

$$L_w/L_b = R_a/R_c.$$

This corresponds to perfect a.c. bridge balance with the terminal points $S_{6,7}$ at minus infinity. If the adjustable inductor is further increased the poles $S_{6,7}$ move to the right half-plane and hence the system could become unstable. Equation

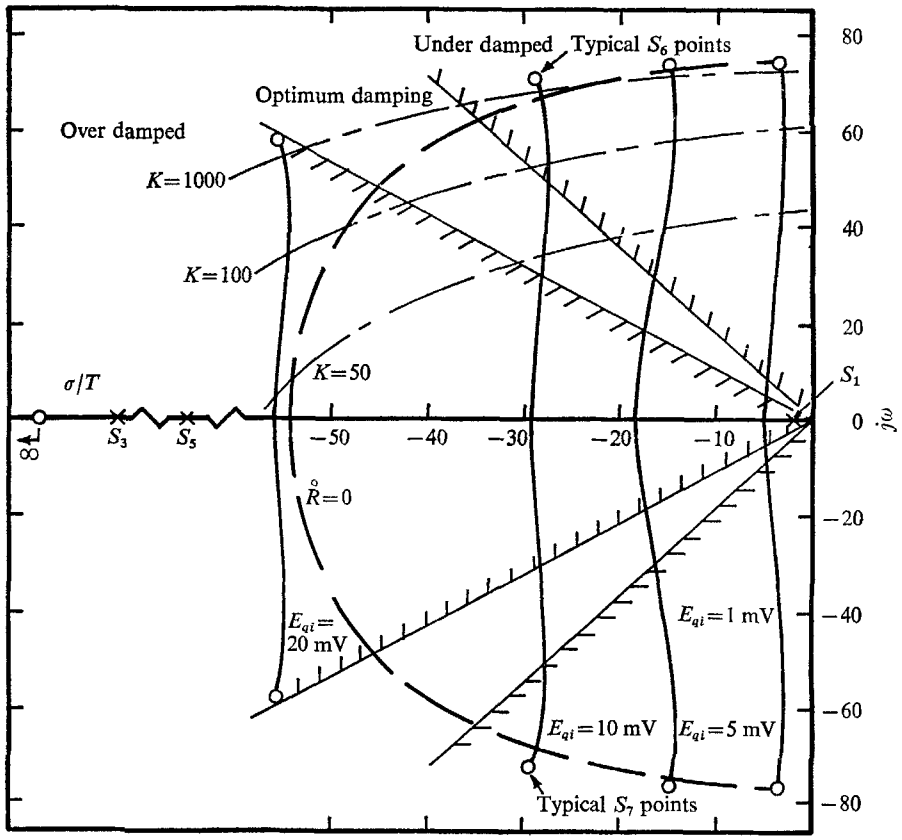

FIGURE 11. S plane loci of operating point for $L_b = 39\ \mu$H. $L_w = 5\mu$H, $\bar{U} = 30\ \text{ms}^{-1}$.

(48) shows that 'over adjustment' of the offset voltage has a similar effect. This instability is not predicted by the analysis with $\mathring{R} = 0$ since the terminal point as derived from the simplified theories are independent of the offset voltage. Although the terminal points may be shifted to infinity by suitable adjustment of L_b, the frequency response of a real system is limited by other stray reactive effects and by the finite response of the feedback amplifier. Although these two factors limit the improvement of the system frequency response, they do not change the instabilities generated by an over adjustment of L_b.

One commercial hot-wire system in common use has a compensating inductor and fixed offset voltage. By suitable adjustment of the inductor the required

damping may be obtained, but an unsatisfactory frequency response may result. Alternatively the inductor may be used to obtain maximum frequency response, but often at the expense of incorrect damping. This system has the advantage of a fixed offset voltage and hence the static calibration remains unchanged for a given wire and resistance ratio. A serious disadvantage of this method is that, under certain conditions, the adjustment of L_b is critical. A slight over adjustment

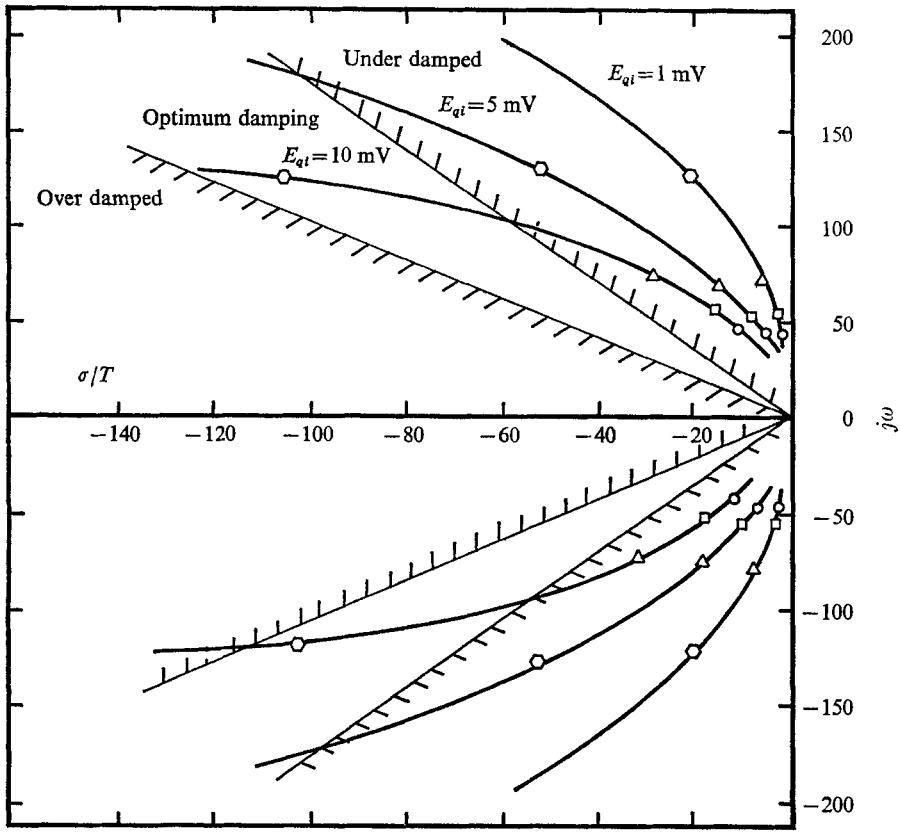

FIGURE 12. S plane trajectories of operating point for varying inductance L_b: ○, 19 μH; □, 29 μH; △, 39 μH; ⬡, 47 μH. L_w = 5 μH, K = 1000, $\bar{U}$ = 30 ms^{-1}.

can cause the system singularities to rapidly 'jump' to the positive half-plane. It must also be possible to vary L_b through a wide range of values if the system is to match the various probes, cables and flow conditions encountered. These difficulties can be overcome by using an adjustable offset voltage. This enables both high-frequency response and optimum damping to be obtained with the inductor remote from its critical value. Offset voltage adjustments can also cater for the various cables and flow conditions. Also, figure 11 indicates that adjustment of the amplifier gain further increases the flexibility of the system from the viewpoint of the operator.

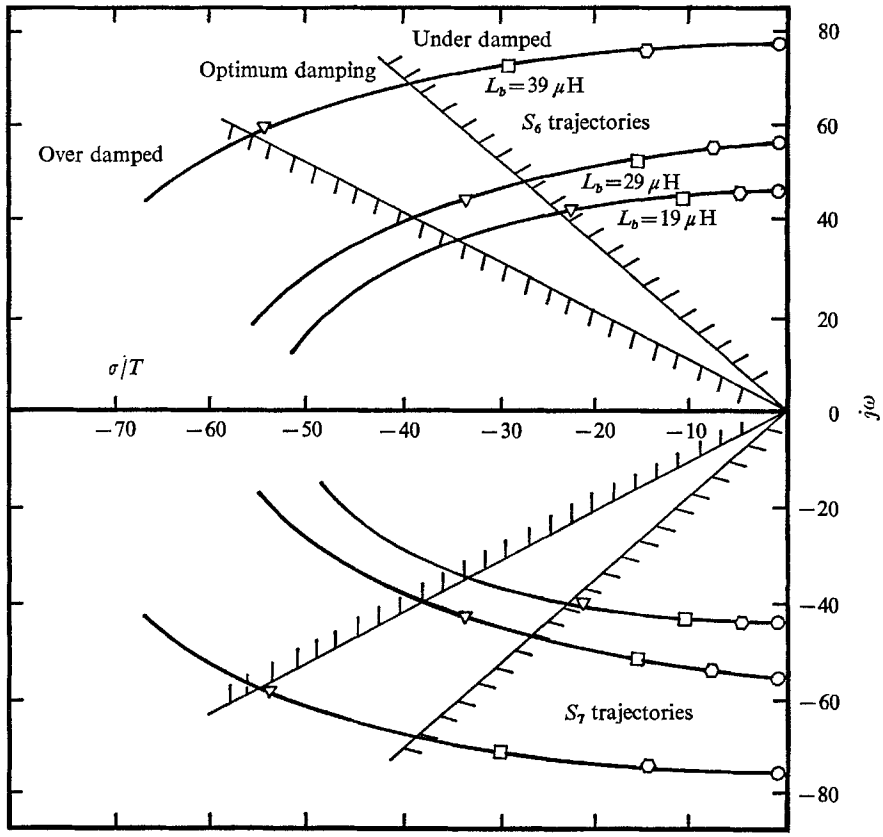

FIGURE 13. S plane trajectories of terminal points for varying offset voltage: ○, 0 mV; ◇, 5 mV; □, 10 mV; ▽, 20 mV. $L_w = 5\mu$H, $\bar{U} = 30\,\text{ms}^{-1}$.

6.4. *Effect of amplifier roll-off on closed-loop frequency response*

Grant & Kronauer (1962) and Freymuth (1967) investigated this problem for the case of an ideal high-gain non-inductive hot wire, ignoring bridge imbalance and interaction between inductance and offset. When the combined effects of simple amplifier lag, wire inductance and bridge imbalance are investigated a third-order response is obtained and the analysis shows that the amplifier response has a secondary effect on the system frequency response compared to the limits imposed by the wire inductance. The instabilities due to amplifier roll-off as discussed by Kovasznay (1948) and Grant & Kronauer (1962) are not applicable to a system with bridge imbalance. For the feedback system analysed in this paper the system frequency response may be much higher than the amplifier open-loop response if the offset is suitably adjusted for optimum response.

6.5. *Effect of amplifier common mode rejection*

In the previous analysis in this paper perfect common mode rejection was assumed. This will not be achieved in practice. To allow for different gains of the

two amplifier inputs both the static and dynamic analyses must be modified; thus (1) becomes

$$E_0 = -K_a E_a + K_b E_b + K E_{qi}, \tag{49}$$

where the points a and b are shown in figure 1, and K_a and K_b represent the two amplifier gains. When the dynamic analysis of the inductive wire of §6.1 is modified to take account of the different gains the transfer function becomes a function of the differential gain error $K_c = K_a - K_b$. The typical system shown in figure 1 becomes unstable if $K_c = -0{\cdot}01\,K_a$. The error in any given system may be allowed for by increasing the offset voltage thus shifting the roots back to the required part of the left-hand plane. However, this may adversely effect the frequency response.

6.6. *Effect of finite amplifier gain*

Section 2 shows that the wire static resistance is a function of the mean velocity, except for zero offset voltage. For fixed E_{qi} the wire resistance asymptotes to a constant resistance R_{wa} as U approaches infinity, as shown in figure 2. The effect of the variation of wire resistance on the dynamic sensitivity may be determined by investigating the calibration procedure.

The conventional calibration procedure is to plot the wire static current, or voltage, squared against $\sqrt{U}$. King's law predicts that when plotted on these axes the data should form a straight line thus:

$$E_0^2 = M + N\sqrt{U}, \tag{50}$$

where $$M = (\bar{R}_w - R_g)P/\bar{R}_w, \quad N = (\bar{R}_w - R_g)Q/\bar{R}_w,$$

P and Q are constants for a given wire and fluid. Ideally (50) shows that the system small-perturbation sensitivity is

$$K_1 = \partial E_0/\partial U = N/4E_0\sqrt{U}. \tag{51}$$

The effect of wire resistance variation with mean velocity is to change N so that the gradient of the calibration curve deviates from the ideal constant-temperature value. Many designers have used high-gain amplifiers to keep the wire resistance as constant as possible, so that the system operation approximates the ideal constant-resistance case, thus eliminating the variations mentioned above. The important factor overlooked in such reasoning is that the deviation of the wire resistance from the ideal constant value depends not only on the amplifier gain but also on the offset voltage. This is also applicable to those systems which have high d.c. gain and moderate a.c. gain. For satisfactory response the offset voltage must be adjusted to give optimum damping somewhere in the range of interest. Consider a system with a wire inductance of $5\,\mu$H and an offset voltage so that optimum response is obtained at $U = 30\,\mathrm{ms}^{-1}$. The extent of the deviation of N from the ideal constant-temperature value is shown in figure 14 for various amplifier gains. Each gain has the required offset voltage for optimum response at $30\,\mathrm{ms}^{-1}$. Although the absolute value of this deviation may be large (typically 5 % for $K = 100$), the curvature of the calibration data is small. For a velocity range of 2 to $30\,\mathrm{ms}^{-1}$ the gradient for $K = 100$ changes by only 1·6 %. In practice the sensitivity of the system is obtained from the gradient

of the straight line of best fit through the calibration points. This corrects for most of the deviation shown in figure 14. The remaining error is introduced by the curvature and this amounts to only $\pm$ 0·8 % for the above conditions. For a gain of 1000 the error is $\pm$ 0·5 % and for a gain of 10000 approximately $\pm$ 0·3 %. Thus if the system is adjusted to have optimum damping only a small improvement of resistance variation is achieved by using amplifier gains beyond a 1000.

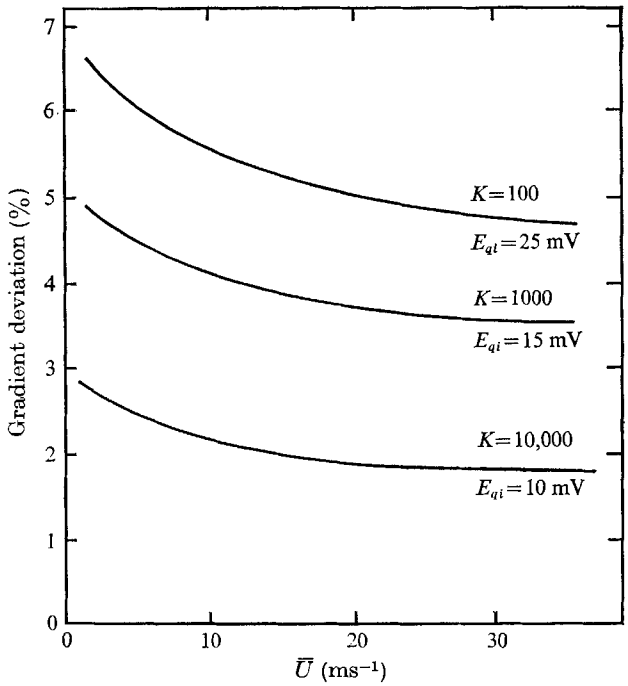

FIGURE 14. King's law doviation from ideal constant-temperature value.

7. Direct experimental determination of system frequency response

Although the characteristic equation for velocity perturbations has been shown to be the same for external voltage excitation, a more satisfactory and convincing demonstration of a system's response is a direct test with velocity perturbations.

Producing a velocity perturbation of fixed amplitude but with variable frequency is difficult. One method is to use the principle of similarity of vortex streets behind cylinders of different size but operating at the same Reynolds number and with the hot wire situated at a fixed number of cylinder diameters downstream.

Such an experiment was performed using a cylinder Reynolds number of 140 in order to obtain a stable single-frequency vortex wake (double frequency at the centreline of the wake). The hot-wire systems used were a Disa 55A01 and a system constructed by the authors. Both systems were separately calibrated using a dynamic calibration procedure developed by the authors. A report of this procedure is being prepared. The same hot wire and probe were used to test both

systems. The wire diameter was 4 μm, wire length 1·2 mm and the mean velocity in all tests was less than 10 ms^{-1}. The results of these tests are summarized in figure 15 which shows the variation of turbulence against frequency. The response of the authors' system was flat to beyond 10 kHz (the maximum frequency attainable) and the Disa response had a 3 db point ($\overline{u'^2}$ reduced by 50%) at 6 kHz. The conventional electronic tests indicated that the response of the former was 30 kHz while the response of the Disa was 5 kHz.

The reason for the poor response of the Disa is that it incorporates a very high d.c. gain amplifier in an attempt to maintain the wire resistance constant for all operating velocities (see § 6.6). In order to achieve stable performance of such a high-gain system over a wide operating range it is necessary to use a high offset voltage which in this case was fixed. This high offset voltage partially nullifies

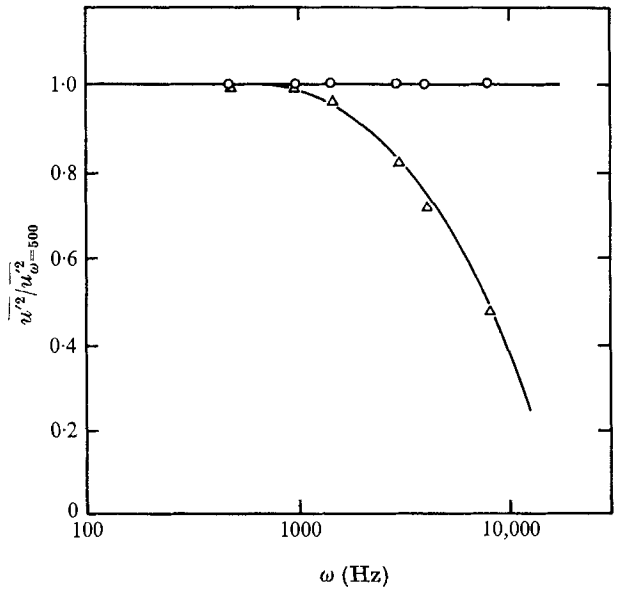

FIGURE 15. Cylinder wake turbulence measurements. ○, authors' hot wire; △, Disa 55 AO 1.

the advantage of high gain (see § 6.6). The model proposed in this paper shows that these conditions produce poor response at low mean velocities, i.e. typical velocities used in boundary-layer research. As the analysis and above experiment show, high-frequency response may be obtained at any mean velocity with optimum damping if the offset voltage is suitably adjusted. A few commercial systems currently available incorporate some offset-voltage control (e.g. Disa 55 DO 1).

8. Discussion and conclusions

The authors believe that the knowledge gained from the analysis presented in this paper is essential not only for designers of hot-wire systems but also for proper use by operators.

Two techniques are examined for setting the desired values of frequency response and damping. First is the widely practised method of using a trimming inductor and fixed offset voltage. If the feedback system is to be used with a range of probes, probe cable lengths and mean velocities, it may operate stably but will have neither optimum damping nor maximum frequency response over the entire design range. Satisfactory response over even part of the range of measurements generally undertaken with a hot wire is difficult to achieve with the first technique, and it is demonstrated here that the adjustment of inductance may be critical under certain conditions. Instability will result if the trimming inductor is taken slightly beyond its optimum setting. This instability may be overcome by using a high fixed offset voltage but this has the disadvantage of producing rather poor frequency response at low mean velocities.

The second technique, which gives more flexibility, is for the operator to have control over the compensating inductor, the offset voltage and the amplifier gain. The recommended procedure for adjusting the system is initially to select the amplifier gain. For subsonic measurements using a platinum or tungsten wire of 4 μm diameter and 1·2 mm long a gain of 500 to 1000 is satisfactory. These gains will produce a frequency response close to the maximum possible. The operator must then decide at which mean velocity to adjust the system for optimum damping. The procedure is to inject a square-wave voltage and iterate between the adjustment of the compensating inductor and offset voltage until a damping coefficient of 0·6 and maximum desired frequency response are obtained. If the system is adjusted for optimum damping at a mean velocity of 20 ms^{-1} it will maintain satisfactory damping over the velocity range 2–40 ms^{-1}. This is satisfactory for most boundary-layer measurements. If the same hot wire were to be used at a much higher mean velocity it would be necessary to re-adjust the offset voltage to suit the new conditions and carry out a new calibration.

The results of the cylinder wake measurements demonstrate the marked improvement in system frequency response and damping that may be achieved by using the second technique.

Analysis of a hot-wire system taking account of wire inductance, bridge imbalance and a simple amplifier lag shows surprisingly that the dominant factor in determining the system frequency response is the bridge inductance and not the amplifier frequency response.

Since the calibration takes account of the major component of the variation of wire temperature as the mean velocity changes, the error introduced by finite amplifier gain in the static I_1^2 *vs.* $\sqrt{U}$ calibration is less than $\pm 0.5\ \%$, until the gain is as low as a few hundred. The previous practice of using very high gain amplifiers to eliminate the wire temperature variation ignores the fact that the variation of wire resistance with velocity depends not only on the amplifier gain but also on the offset voltage. If the system offset is adjusted to give optimum damping, little improvement in wire resistance variation is achieved by using very high gain amplifiers. Alternatively if low offset voltages and high amplifier gains are used to approach the ideal constant-temperature operation, the system operates in a range where the trimming inductor adjustments become critical and a range of inductors are necessary to suit various operating conditions. Since

the stability of the system is the most important factor the second scheme is preferred despite the slight variations of wire resistance and the necessity to recalibrate after each adjustment of the offset voltage.

The authors are indebted to the Australian Institute of Nuclear Science and Engineering for financial support of this project.

REFERENCES

ANDERSON, O. 1966 *Disa Information*, unpublished report, **4**, 3.

BERGER, E., FREYMUTH, P. & FROBEL, E. 1963*a* *Deutsche Versuchsanstalt für Luft- und Raumfahrt*, no. 282.

BERGER, E., FREYMUTH, P. & FROBEL, E. 1963*b* *Konstruktion*, **15**, 495.

DAVIS, M. & DAVIES, P. 1968 *Univ. of Southampton*, ISVR. TR2.

FREYMUTH, P. 1966 *Deutsche Versuchsanstalt für Luft- und Raumfahrt*, no. 66–03.

FREYMUTH, P. 1967 *Rev. Sci. Instrum.* **38**, 677.

GRANT, H. & KRONAUER, R. 1962 *Symposium on Measurement of Unsteady Flow*, p. 44. ASME. Hydraulic Division Conference. Worcester, Mass.

HINZE, J. 1959 *Turbulence: an Introduction to its Mechanism and Theory*. McGraw-Hill.

HOROWITZ, I. 1963 *Synthesis of Feedback Systems*. Academic.

JANSSEN, J., ENSING, L. & VAN VERP, J. 1959 *Proc. I.R.E.* **47**, 555.

KOVASZNAY, L. S. G. 1948 *Johns Hopkins Univ.* Aero CM-478.

OSSOFSKY, E. 1948 *Rev. Sci. Instrum.* **19**, 881.